Catalysis Science & Technology

PAPER

Cite this: DOI: 10.1039/c4cy01237b

Synthesis of glycerol carbonate by direct carbonylation of glycerol with CO_2 over solid catalysts derived from Zn/Al/La and Zn/Al/La/M (M = Li, Mg and Zr) hydrotalcites†

Hongguang Li,[ab] Xi Jiao,[ab] Lei Li,[a] Ning Zhao,*[a] Fukui Xiao,[a] Wei Wei,[c] Yuhan Sun[d] and Bingsheng Zhang[e]

Received 23rd September 2014,
Accepted 18th October 2014

DOI: 10.1039/c4cy01237b

www.rsc.org/catalysis

Zn/Al/La and Zn/Al/La/M (M = Li, Mg, Zr) mixed oxides were obtained by calcination of hydrotalcite precursors and tested for glycerol carbonate (GC) synthesis from CO_2 carbonylation. The results indicated the catalytic activity may be associated with the large specific surface area, the high surface content of Zn and the high binding energy of Zn atoms as well as the high density of moderately basic sites. The good result was obtained on the catalyst with a molar ratio of Zn : La : Al = 4 : 1 : 1 and, within a certain range, glycerol conversion and GC yield increase linearly upon the increase of the density of moderately basic sites. In addition, the catalytic activity was obviously improved upon introduction of Li, Mg and Zr. The effect of reaction parameters on the carbonylation of glycerol was also studied. The DRIFTS results suggest that the activated CO_2 may be in the form of a bridged bidentate carbonate that inserts into zinc glycerolate to form an intermediate species of a seven-membered ring ester followed by intramolecular rearrangement to produce GC. Theoretical calculation results indicated that the seven-membered ring ester has good stability and the formation process happens spontaneously.

1. Introduction

The mixture of fatty acid methyl esters (FAMEs), known as biodiesel, which can significantly decrease the emission of CO_2, SO_x and unburned hydrocarbons from motor vehicles,[1] has received much attention and as a result, its production has increased greatly in recent years. However, a large amount of glycerol has also been produced as a byproduct. Worldwide, the production of glycerol is in a surplus which has resulted in the market price of glycerol dropping sharply.[2–4] Consequently, new applications for the low-cost glycerol need to be developed and/or the existing routes need to be expanded.[2] Recently, new pathways for the catalytic conversion of glycerol, including selective oxidation, selective hydrogenolysis, selective dehydration, thermal reduction into syngas, selective etherification and synthesis of glycerol carbonate (GC), have been developed.[3–5] Glycerol carbonate, an important glycerol derivative, can be widely used as a novel component of gas separation membranes, polyurethane foams, surfactant as well as the component in coatings, paints and detergents, *etc.*[5,6] Therefore, synthesis of glycerol carbonate from glycerol becomes very meaningful.

Traditionally, GC was prepared by reaction of glycols with phosgene. Due to the high toxicity and corrosive nature of phosgene, alternative routes such as transesterification of dialkyl or alkylene carbonates have been explored.[7–13] However, the transesterification process involves dimethyl, diethyl or propylene carbonates, which leads to lower economic benefits. Although many heterogeneous catalysts showed good catalytic activity for GC synthesis from glycerol and urea,[9,14–16] the reaction must be conducted at a pressure below 20–30 mbar in order to remove the formed ammonia. Moreover, the purification process is also complicated.[17]

Compared with the above-mentioned synthesis routes, the carbonylation of glycerol with CO_2 is a green process that would convert two cheap raw materials into a valuable product with only water as byproduct. The first attempts to synthesize GC from glycerol and supercritical CO_2 were carried out using zeolites and basic ion-exchange resins as

---

[a] *State Key Laboratory of Coal Conversion, Institute of Coal Chemistry, Chinese Academy of Sciences, Taiyuan 030001, China. E-mail: zhaoning@sxicc.ac.cn*
[b] *University of Chinese Academy of Sciences, Beijing 100049, China*
[c] *Center for Greenhouse Gas and Environmental Engineering, Shanghai Advanced Research Institute, Chinese Academy of Sciences, Shanghai, 201210, China*
[d] *Low Carbon Conversion Center, Shanghai Advanced Research Institute, Chinese Academy of Sciences, Shanghai 201210, China*
[e] *Shandong ACID Chemicals Co., LTD, Feicheng 271600, China*

† Electronic supplementary information (ESI) available: Supporting figures are presented for exploration of the prepared catalysts and experimental results. See DOI: 10.1039/c4cy01237b

catalysts and the GC yield could reach 32%.[18] However, there is no evidence that a direct CO_2 insertion occurred, as only glycerol carbonate was produced when another organic carbonate was added as reactant.[16] The direct reactions of glycerol with CO_2 were also studied using tin complexes, CeO_2/Al_2O_3 or CeO_2/Nb_2O_5, as catalysts.[19–21] Low conversion of glycerol was obtained because of thermodynamic limitations. In order to lift the thermodynamic limit, acetonitrile was used as a coupling agent, and achieved enhanced results.[22–24] Although many research works have been reported, it is still a challenge to develop new catalysts with better performance for the synthesis of GC from CO_2.

It is reported that the mixed metal oxides, obtained by calcination of the hydrotalcite-like compounds (HTlcs) ($[M^{2+}{}_{1-x}M^{3+}{}_x(OH)_2]^{x+}(A^{n-})_{x/n}\cdot mH_2O$), possess an homogeneous dispersion of M^{2+} and M^{3+} at an atomic level, high specific surface area and strongly basic properties,[25–27] and the acid–base properties of the catalysts can be modified by changing the cations in the layers, compensating anions or activation methods.[28] As a result, they have been studied for various catalytic reactions including the synthesis of GC by transesterification or carbonylation with urea.[8–10,13,29] In addition, some researchers have reported that zinc-based catalysts have a strong ability for glycerol activation,[14,15,29–31] and lanthanides favor metal dispersion and strengthen CO_2 adsorption.[32] To the best of our knowledge, the use of La modified zinc-based catalysts derived from HTlcs for the synthesis of GC from glycerol and CO_2 has not been reported before.

In the present work, Zn/La containing hydrotalcites (Zn–Al–La and Zn–Al–La–M (M = Li, Mg and Zr)) are prepared and their catalytic activities for the synthesis of GC from glycerol and CO_2 are investigated for the first time. The influence of the introduction of La to the Zn/Al HTl structure, the Al content and different metal elements (Li, Mg and Zr) into the layered structure on the physicochemical properties are discussed. The relationship between the physicochemical properties and the catalytic performance is then discussed. CO_2 adsorption on the prepared catalysts and the interaction between zinc glycerolate and CO_2 are studied by DRIFTS. The used catalysts are studied by FT-IR. The possible mechanism for glycerol carbonate synthesis was thus proposed and theoretical calculations are also performed with the Gaussian 09 program to verify the proposed mechanism.

2. Experimental

Catalyst preparation

La modified Zn-containing HTlcs with various Zn : La : Al atomic ratios were synthesized by a co-precipitation method. The $Zn^{2+} : La^{3+} : Al^{3+}$ atomic ratio in the starting solution was kept to 4 : 1 : x where x was varied from 1 to 3. Typically, two aqueous solutions, a solution of Zn(II), Al(III) and La(III) nitrates and a mixed solution of NaOH and Na_2CO_3 precipitant, were added dropwise to 100 mL of deionized water under vigorous stirring with a constant pH of 10. The resulting slurry was aged at 60 °C for 15 h under stirring and then filtered and washed several times with deionized water until the filter liquor reached a pH value of 7. Thus obtained solids were dried at 80 °C overnight and then calcined in air at 500 °C for 5 h with a heating-up rate of 5 °C min^{-1}. The obtained HTlcs were denoted as HT-x (x means the $Al^{3+} : La^{3+}$ atomic ratio in the synthesis mixture), and corresponding calcined HTlcs were denoted as CHT-x.

The same methodology was used for the preparation of Zn/Al/La/M (Zn/Al/La/M = 4 : 1 : 1 : 1, M = Li, Mg, Zr), Zn/Al ($Zn^{2+} : Al^{3+}$ = 2 : 1) hydrotalcites and the catalyst of $Zn^{2+} : La^{3+}$ = 4 : 1, which were denoted as HT-M, ZA-2, ZL-4 (before calcination) and CHT-M, CZA-2, CZL-4 (calcined at 500 °C), respectively. Furthermore, zinc glycerolate was prepared by the reported method[33] for the exploration of the interaction with CO_2 to understand the mechanism of the formation of glycerol carbonate.

Characterization of catalysts

The surface area of the samples was determined by N_2 adsorption–desorption at −196 °C on Micromeritics Tristar 3000 instrument. X-ray diffraction (XRD) patterns were recorded on Panalytical X'Pert Pro X-ray diffractometer with Cu Kα radiation over a range of 10–80°. Thermogravimetric analysis (TGA) was performed on a Rigaku thermogravimetric analyzer with 60 mL min^{-1} of air flow from 30 to 800 °C at a heating rate of 10 °C min^{-1}. The morphology of the samples was determined on a JEOL JSM-7001F scanning electron microscope (SEM) with an accelerating voltage of 10.0 kV.

X-Ray photoelectron spectroscopy (XPS) measurements were performed over a Kratos AXIS ULTRA DLD spectrometer equipped with Al Kα radiation ($h\nu$ = 1486.6 eV) under ultrahigh vacuum. The binding energies were calibrated internally by adventitious carbon deposition C (1s) with E_b = 284.8 eV.

The surface basicity of the catalysts were measured by temperature programmed desorption of CO_2 (CO_2-TPD) using a TPD flow system equipped with an MS detector (Omnistar, PFEIFFER VACUUM). Each sample (0.1 g) was pre-treated in Ar flow at 500 °C. The adsorption of CO_2 was performed at 40 °C and then followed by an Ar purge to remove the physisorbed CO_2. The desorption process was performed at a heating rate of 10 °C min^{-1} from 40 °C to 500 °C.

CO_2 adsorption was explored by a diffuse reflection infrared Fourier transform spectroscopy (DRIFTS) experiment with a Nicolet Magna-II 550 spectrometer. The sample was heated to 400 °C in Ar flow and held at this temperature for 1 h prior to experiment in order to remove absorbed gas and water. 100 scans were recorded after it cooled to 170 °C. High-purity carbon dioxide was introduced to the cell at 50 mL min^{-1} for 1 h. Recording of the spectra of CO_2 adsorption was followed by sweeping with a flow of 50 mL min^{-1} of Ar for 5, 10, 20 and 30 min. 100 scans of adsorbed CO_2 were recorded at a resolution of 8 cm^{-1}.

The interaction between zinc glycerolate and CO_2 was also explored by DRIFTS experiments on the Nicolet Magna-II 550.

Zinc glycerolate was loaded into the DRIFTS cell and 100 scans were recorded when high-purity CO_2 was introduced to the cell at 60 mL min^{-1}. The corresponding spectra were recorded after 15 min reaction at each temperature point (30, 60, 80, 100, 120, 140, 150, 160, 170, 180 and 190 °C). For comparison, the spectra of zinc glycerolate and glycerol carbonate were also recorded on the spectrometer.

The Fourier Transform Infrared spectra (FT-IR) of the used catalysts were obtained using a Nicolet NEXUS 470 FT-IR spectrometer by the KBr disc method over a range of 400–4000 cm^{-1} with a 4 cm^{-1} resolution.

Evaluation of catalysts

The GC synthesis was carried out in a 50 mL stainless-steel autoclave equipped with a magnetic stirrer. In a typical experiment, glycerol (4.60 g), the desired amount of catalyst (0.14 g, 3 wt% of glycerol) and 5.0 mL CH_3CN were added into the reactor. Then CO_2 was introduced into the autoclave with an initial pressure of 4.0 MPa at 20 °C. The reactor was then heated to 170 °C and kept for 12 h with magnetic stirring. After reaction, the autoclave was cooled to room temperature and the excess CO_2 was vented slowly. For quantitative analysis, an external standard of acetonitrile was used. Considering the low solubility of glycerol and the products in acetonitrile and the high solubility in ethanol, ethanol was also added to dilute the reaction mixtures. Then the samples were analyzed by a gas chromatograph equipped with a flame ionization detector on a capillary column SHIMADZU CBP/20 (25 m × 0.22 mm).

Theoretical methods

Theoretical calculations were used to explore the reaction mechanism. All calculations were carried out with the Gaussian 09 program.[34] Full geometry optimizations were performed at the MP2(Full)/aug-cc-pVDZ level. Harmonic vibrational frequencies were then computed using the same method to confirm that the obtained structures were stable. The Δ_rG was calculated as the difference in the energy between the reactants and products.

3. Results and discussion

Textural properties of the prepared catalysts

The XRD patterns of HT-*x*, ZA-2 and ZL-4 are shown in Fig. 1a. The HTl structure is not formed on the catalyst of ZL-4, and $La(OH)_3$ is the main crystal phase. For ZA-2, only the diffraction peaks of HTlcs are observed. In addition, for La-containing hydrotalcites, the crystallinity of the HTlcs increases upon increase of Al content, reaching a maximum for HT-2 and then decreases with further increase of Al content. The results suggest that a greater amount of hydrotalcite-like structures are formed in HT-2, which is also confirmed by the SEM results (Fig. S1†). The morphologies of the Zn/Al/La precursors in Fig. S1† show that the crystallinity of the HTl structure decreases with the introduction of La, while HT-2 shows high crystallinity of the HTl structure. Previous reports suggested that an atomic ratio of M^{2+}/M^{3+} between 2 to 4 was favorable for the synthesis of the HTl structure.[35,36] As a result, a lower atomic ratio of M^{2+}/M^{3+} in HT-3 (Zn^{2+}/Al^{3+} = 1.3) is not favorable for the formation of single phase HTl structures, so the intensity of the diffraction peaks of the HTl structure decreases for the HT-3 sample.

For the La-containing HTlcs, besides the major phase of the HTl structure, the patterns of $LaCO_3OH$ (JCPDS 26-815) and ZnO (JCPDS 36-1451) are also observed. Benito *et al.*[37] have reported that it is impossible to hinder ZnO segregation in Zn/Al HTlcs when the Zn^{2+}/Al^{3+} atomic ratio was higher than 2. So, the appearance of ZnO diffraction peaks in HT-1 may result from the high atomic ratio of Zn^{2+}/Al^{3+}. Moreover, despite the same atomic ratio of Zn^{2+}/Al^{3+} in ZA-2 and HT-2, the appearance of the diffraction peaks of ZnO in HT-2 may be ascribed to the introduction of La, which is not favorable for the formation of the HTl structure. However, the diffraction peaks of ZnO disappeared in HT-3, which may exist in an amorphous state.

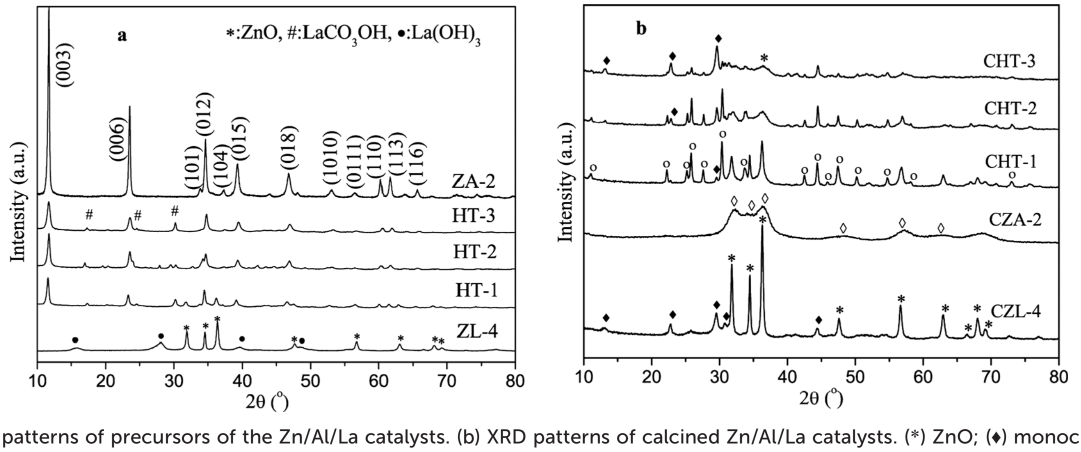

Fig. 1 (a) XRD patterns of precursors of the Zn/Al/La catalysts. (b) XRD patterns of calcined Zn/Al/La catalysts. (*) ZnO; (♦) monoclinic $La_2O_2CO_3$ (JCPDS 48-1113); (○) hexagonal $La_2O_2CO_3$ (JCPDS 37-804); (◊) $Zn_6Al_2O_9$ (JCPDS 51-37).

The unit cell parameters *a* and *c* are calculated by using the reported method[38] and the results are listed in Table 1. It can be seen that both the lattice parameters *a* and *c* increase with the introduction of La. The increase of parameter *a* can be attributed to the isomorphous substitution of Al^{3+} (ionic radius 0.053 nm) in the octahedral sites by La^{3+} (ionic radius 0.103 nm),[39,40] which is in accordance with the FTIR results of the Zn/Al/La HTls (Fig. S2†). The parameter *c*, corresponding to interlayer separation, increases from 22.65 to 22.84 Å with the introduction of La which might be ascribed to the following reasons. Firstly, La prefers to locate in the interlayer gallery of HT as separate hydroxide and hydroxyl carbonate phases which result in the decrease of the electrostatic attraction between the layers and the interlayer anions, leading to the increase of the layer spacing.[38] Moreover, the spacing between the HTl layers might increase if a smaller cation (Al^{3+}) is substituted by a larger cation (La^{3+}).[39,40]

Fig. 1b shows the XRD patterns of CHT-*x*, CZA-2 and CZL-4. It is observed that upon thermal decomposition at 500 °C, the HTl structure collapses and forms the corresponding metal oxide/carbonate. With the increase of Al content, the peak intensity of ZnO decreases and broadens, suggesting that the ZnO particle size becomes smaller. Besides, $La_2O_2CO_3$ experiences a crystal transformation from hexagonal to monoclinic. Diffraction peaks ascribed to Al_2O_3 are not found in the calcined catalysts, indicating that Al_2O_3 may exist in an amorphous state. For the CZA-2 catalyst, no other crystalline phases are observed except $Zn_6Al_2O_9$ (JCPDS 51-37). In addition, ZnO and monoclinic $La_2O_2CO_3$ are the main crystal phases in the CZL-4 catalyst.

The specific surface area and pore volume of the calcined samples are listed in Table 1. Prescott *et al.*[41] and Meher *et al.*[42] have reported that a high content of Al_2O_3 in the catalysts is favorable to increase the specific surface area. Similar results are found on Zn/Al/La samples, *e.g.* an increase Al content leads to a marked increase in the BET surface area from 36.4 to 168.3 $m^2\ g^{-1}$. Pore volume also increases with increase of Al content. As described by Cantrell *et al.*,[43] Al favors higher CO_3^{2-} contents in the interlayer, therefore more open porous networks are produced after thermal treatment. By comparing the samples of CZA-2 ($Zn^{2+}/Al^{3+} = 2$) and CHT-1 ($Zn^{2+}/(Al^{3+} + La^{3+}) = 2$), it is found that the introduction of La leads to the decrease of specific surface area.[38] In addition, the lowest surface area of CZL-4 can be ascribed to the formation of large particles (see SEM profiles) which is not favorable for the exposure of more active sites.

Table 1 Texture properties and crystallographic parameters of prepared catalysts[a]

Sample	Unit cell parameters (XRD)/Å *a*	*c*	Surface area of calcined samples/$m^2\ g^{-1}$	Pore volume of calcined samples/$cm^3\ g^{-1}$
ZL-4	—	—	20.6	0.14
ZA-2	3.069	22.65	62.5	0.082
HT-1	3.078	22.84	36.4	0.069
HT-2	3.073	22.68	79.5	0.29
HT-3	3.073	22.65	168.3	0.19
HT-Li	3.078	22.73	47.4	0.20
HT-Mg	3.078	22.87	82.5	0.45
HT-Zr	3.080	22.96	26.4	0.10

[a] The unit cell parameters *a* and *c* were calculated from the peak position of (110), (003) and (006) reflections by using the formulas: $a = 2d_{(110)}$ and *c* (basal spacing between the layers) = $3/2[d_{(003)} + 2d_{(006)}]$.

The morphologies of the prepared materials calcined at 500 °C for 5 h are shown in Fig. 2. It can be seen that the large particle size in CZL-4 (Fig. 2A) should be responsible for its small surface area (Table 1). The aggregated plate-shaped crystals are also observed in CZA-2, CHT-1 and CHT-2. The small particles appeared in CHT-1 and CHT-2 also indicates that the introduction of lanthanum is not favorable for the synthesis of HTl structure, which is in accordance with the XRD results. In addition, the amount of small particles decreases with the increase of Al content for CHT-*x* catalysts, reaching a minimum for CHT-2 (see Fig. 2D) and then increases with further increase of Al content. Small particles become the main morphology for CHT-3 (see Fig. 2E) which is in accordance with the results of the morphology change in HT-*x* catalysts (Fig. S1†). The most likely explanation for the change is that a suitable molar ratio of Zn/Al is essential for the formation of the HTl structure, which is consistent with the XRD results and previous reports.[35,36] Moreover, more small particles in CHT-3 result in the increasing of BET surface area.

Fig. 3 presents the TG profiles of the prepared samples. For ZL-4, the three major weight losses can be ascribed to the elimination of physically adsorbed water (around 95 °C), the decomposition of lanthanum carbonate (around 310 °C) that forms $La_2O_2CO_3$, and the decomposition of $La_2O_2CO_3$ that forms La_2O_3 (about 640 °C), respectively.[44,45]

The TG curves of HTlcs consists of three weight losses: the elimination of physically adsorbed or interlayer water molecules (100–200 °C), the removal of both the hydroxyl groups from the HTl network and the carbonate anions from the interlayer anion (200–340 °C), and the decomposition of metal carbonates (380–630 °C) formed during the former steps of the thermal decomposition. Furthermore, another weight loss is also found at around 690 °C in HT-*x* catalysts, which may be ascribed to the decomposition of $La_2O_2CO_3$.

The weight losses of the prepared catalysts are compared in Table 2. For HT-*x* catalysts, the second and third weight losses reach the maximum for HT-2, suggesting that more HTlcs are formed. In addition, the TG profiles show that the introduction of La^{3+} results in a decreasing of the decomposition temperatures, especially for the third step (*e.g.*, ZA-2: 600 °C; HT-3: 462 °C; HT-2: 458 °C; HTs-3: 446 °C). Furthermore, compared with ZA-2, the second step in HT-*x* catalysts also shifts to lower temperatures. The results reflect a gradual decrease of the thermal stability of the catalysts. It can be ascribed to the presence of separated lanthanum hydroxide and hydroxyl carbonate phases in the interlayer space, which

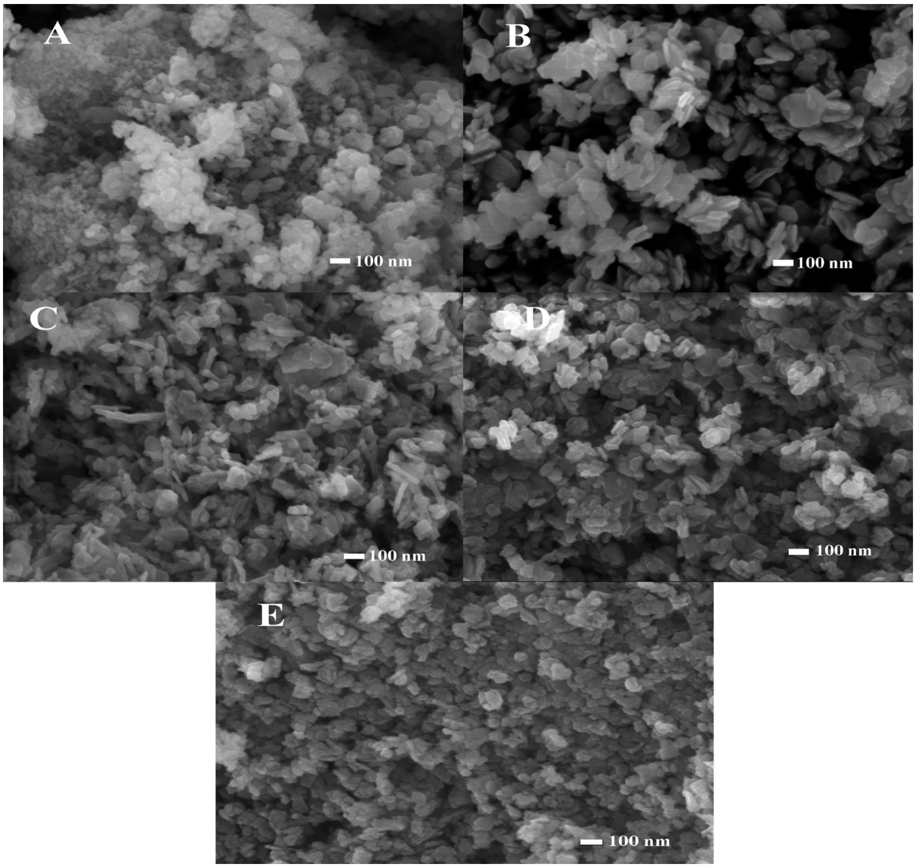

Fig. 2 SEM images of different samples: (A) CZL-4, (B) CZA-2, (C) CHT-1, (D) CHT-2, (E) CHT-3.

lead to a decrease of the electrostatic attraction between the layers and the interlayer anions[38] that results in the increase of the interlayer space and lower thermal stability.

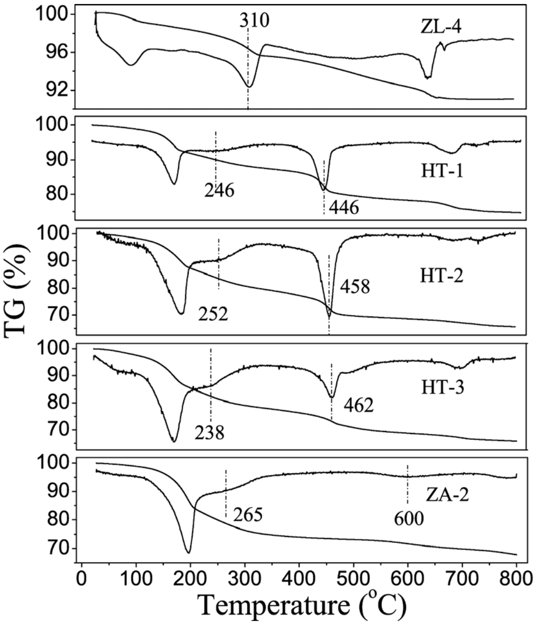

Fig. 3 TG-DTG analysis of ZA-2, ZL-4 and HT-*x* catalysts.

XPS investigations

The oxides of Zn/Al/La catalysts are analyzed by XPS, and the binding energies (BE) of Zn $2p_{3/2}$ and La 3d are presented in Table 3. For all samples, XPS peaks are found at around 834.2–834.7 eV (BE) for La 3d. The Zn $2p_{3/2}$ peak at 1020.6–1021.9 eV can be assigned to the Zn^{2+} species on the catalyst surface. The highest BE of Zn $2p_{3/2}$ in CZA-2 can be ascribed to the formation of $Zn_6Al_2O_9$ which leads to the formation of strong interaction between Zn, Al and O. For CZL-4 and CHT-*x* catalysts, the BE of Zn $2p_{3/2}$ and La 3d decrease with the increase of Al content, especially for CHT-3, while the BE of Al 2p decreases first and then increases for CHT-*x* catalysts. The results reveal the complex interactions between Zn, La, Al and O atoms.

The surface compositions of the catalysts, as determined by XPS, are shown in Table 3. It is found that the surfaces

Table 2 Weight loss of different stage of ZA-2, ZL-4 and HT-*x* catalysts

	Weight loss (%)			
Sample	First	Second	Third	Fourth
ZL-4	1.0	3.3	4.7	—
ZA-2	15.2	11.1	4.2	—
HT-1	7.5	5.0	8.7	3.7
HT-2	12.5	8.5	10.0	3.5
HT-3	14.0	7.6	8.5	3.8

Table 3 Binding energy and surface composition of different samples

	Binding energy/eV			Surface percentage (at.%)				Surface atom ratio
Sample	Zn $2p_{3/2}$	La 3d	Al 2p	Zn	Al	La	M	$Zn^{2+}:Al^{3+}:La^{3+}$
CZA-2	1021.7	—	74.1	23.3	8.3	—	—	2.8 : 1 : —
CZL-4	1020.9	834.7	—	23.6	—	6.9	—	3.4 : — : 1
CHT-1	1020.8	834.4	74.6	17.9	4.4	3.8	—	4.7 : 1.2 : 1
CHT-2	1020.8	834.3	73.7	16.2	6.6	2.8	—	5.8 : 2.3 : 1
CHT-3	1020.6	834.2	73.9	17.6	9.1	1.6	—	11.0 : 5.7 : 1
CHT-Li	1021.6	834.6	74.1	18.9	5.2	1.3	10.9	14.5 : 4 : 1
CHT-Mg	1021.4	834.6	73.9	13.0	4.9	4.2	0.2	3.1 : 1.2 : 1
CHT-Zr	1021.6	834.8	74.0	17.7	5.4	2.1	2.7	8.4 : 2.6 : 1

M represents Li, Mg and Zr in CHT-Li, CHT-Mg and CHT-Zr, respectively.

are depleted considerably of La and enriched in Zn and Al, except for CZL-4. In addition, the actual value of the atomic ratios of Zn and La are higher than the theoretical value for CHT-*x* catalysts, and the degree of deviation increases upon the increase of the Al content, especially for CHT-3, which can be explained as follows. On the one hand, as described by previous reports,[40,46] Zn prefers to aggregate on the surface of the catalysts. On the other hand, the atomic ratio of M^{2+}/M^{3+} (Zn^{2+}/Al^{3+}) in CHT-3 is not suitable for the formation of the HTl structure,[35,36] which leads to the enrichment of Zn on the surface, and then results in a higher degree of deviation of the Zn/La ratio. Moreover, the percentage of Zn content on the surface of CHT-*x* decreases with increasing of Al content, especially for CHT-2, which can be ascribed to the formation of a higher amount of aggregated plate-shaped crystals (see Fig. 2D) that results in a reduced exposure of Zn atoms.

The basicity of the catalysts

The basicity of the catalysts was measured by CO_2-TPD (Fig. 4). According to previous reports,[36,47,48] CO_2 desorption peaks can be roughly divided into three regions, *e.g.* the weakly (50–150 °C), moderately (200–400 °C) and strongly (>400 °C) basic sites. All profiles in Fig. 4 can be deconvoluted into two Gaussian peaks assigned to weakly and moderately basic sites. CZL-4 shows small amount of weakly basic sites and more moderately basic sites derived from the formation of $La_2O_2CO_3$ according to previous reports.[45,49] In addition, the amount of weakly basic sites increases with the increase of Al content, which can be assigned to the increase of the amount of OH^- groups.[36,50] Compared with ZA-2, the CHT catalysts shows more moderately basic sites with increasing Al content which can be explained as follows:

The increase in the specific surface area could account for the increase of the basicity.[40,50] Despite the higher specific surface area for CZA-2 than CHT-1, more moderately basic sites in CHT-1 can be formed with the formation of $La_2O_2CO_3$. In addition, the amount of metal–oxygen pairs (such as Zn–O, Al–O and La–O) related to the moderately basic sites for metal oxides[50] increases with the increase of Al content within the unit mass because of the smaller molar mass of Al. Moreover, the desorption temperature of moderately basic sites shifts to lower temperatures with the increase of Al content, which suggests that a greater amounts of Al content results in the decrease of moderately basic intensity.

Catalytic performance of CHT-*x* catalysts for GC synthesis

The catalytic performances of the Zn/Al/La catalysts are summarized in Table 4. Acetonitrile was employed since previous reports suggested that it is an effective coupling agent for the process.[22–24,49] Monoacetin and diacetin generated from the reaction of glycerol and acetic acid obtained by the hydrolysis of acetonitrile are detected.[49] Although the formation of acetins as byproducts cannot be avoided, the wide applications of the byproducts may reduce the cost of the synthesis route, *e.g.* monoacetin can be used in the manufacture of dynamite and tanning leather, as a solvent for various dyes,

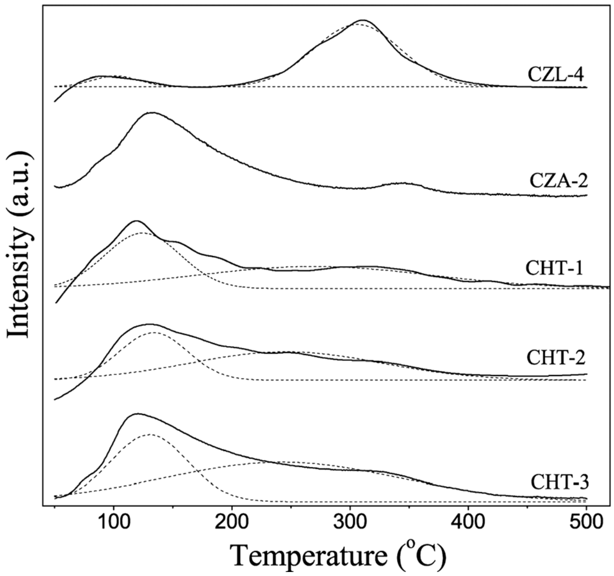

Fig. 4 CO_2-TPD profile of CZA-2, CZL-4 and CHT-*x* catalysts. The values of the second peak area of CZL-4, CZA-2, CHT-1, CHT-2 and CHT-3 were multiplied by 10^{10} and the results are 1.983, 0.252, 3.019, 3.707 and 8.632 (a.u.) g^{-1}, respectively.

Table 4 The catalytic activities of prepared catalysts for GC synthesis from CO_2 and glycerol

Sample	Glycerol conversion (%)	Selectivity (%)			GC yield (%)
		Monoacetin	Diacetin	GC	
CZA-2	23.2	49.4	5.5	45.1	10.4
CZL-4	25.1	50.5	6.2	43.2	10.8
CHT-1	30.4	50.9	5.2	43.8	13.3
CHT-2	29.2	50.7	6.5	42.8	12.5
CHT-3	27.2	52.7	6.9	40.3	10.9
Used CHT-1	23.9	46.5	—	53.5	12.8
CHT-Li	35.7	52.2	5.6	42.2	15.1
CHT-Mg	33.9	51.9	7.7	40.4	13.7
CHT-Zr	32.7	49.8	7.0	43.3	14.1
Li_2CO_3[a]	24.3	55.3	5.1	39.6	9.6
MgO[a]	5.3	100	—	—	—
ZrO_2[a]	1.2	100	—	—	—

Reaction conditions: glycerol 4.60 g, CH_3CN 5.0 mL, catalyst 0.14 g, initial pressure P_{CO_2} = 4.0 MPa, 170 °C, 12 h.[a] Catalyst 0.23 g.

as a food additive, a plasticiser and a softening agent,[51] while diacetin can be used as a solvent, softening agent and fuel additive for viscosity reduction.[52]

Compared with CZA-2, the higher glycerol conversion and GC yield as well as lower GC selectivity on CZL-4 may be associated with a greater amount of moderately basic sites which improve both CO_2 activation[53] and acetonitrile hydrolysis.[22] As a result, greater amounts of acetic acid are formed which lead to a high selectivity for acetins and a low selectivity for GC. CHT-*x* catalysts exhibited better catalytic performance than CZL-4 and CZA-2. A maximum GC yield of 13.3% with a glycerol conversion of 30.4% and GC selectivity of 43.8% is obtained over CHT-1. In addition, the higher selectivity of acetins than GC can be ascribed to the water contained in the reagents of glycerol and acetonitrile, which were analytical agents; there was no dehydration processing and similar results were obtained in the previous report.[54]

On the one hand, compared with CZA-2, the introduction of $La_2O_2CO_3$ improved the surface basicity, which plays an important role in CO_2 activation and acetonitrile hydrolysis.[22,53] On the other hand, the obtained mixed metal oxides derived from the HTl structure have a larger specific surface area, which favors the exposure of more active sites that improve the catalytic activity. However, in association with the results in Table 1, CHT-1 with a moderate surface area exhibited a higher catalytic activity than CHT-2 and CHT-3, suggesting that the catalytic activity is not correlated simply with the specific surface area. The decrease of the catalytic activity can be ascribed to the following reasons: firstly, because ZnO has a strong ability to activate glycerol,[29,31] the decrease of surface Zn content with increasing of Al content leads to a low catalytic activity. In addition, according to the XPS results, zinc shows a higher valence state in the CHT-1 sample, which favors the activation of glycerol and thus improves the catalytic activity.[29,49] Moreover, although the amount of moderately basic sites increases with the increase of Al content (Fig. 4), the large specific surface area of CHT-2 and CHT-3 also leads to a low density of moderately basic sites. Fig. 5 shows that within a certain range, glycerol conversion and GC yield increase linearly upon increasing the density of moderately basic sites, which is probably due to more activated CO_2 as well as the promoted hydrolysis of CH_3CN over basic sites.[22] Therefore, the low catalytic activities of CHT-2 and CHT-3 can be ascribed to the low density of moderately basic sites. Despite the high density of moderately basic sites on CZL-4, the low specific surface area (Table 1) may responsible for its low catalytic activity.[49] Furthermore, it seems that the good activity of CHT-*x* catalysts may also be associated with the CO_2 adsorption species (see the reaction mechanism discussion section). The bridged bidentate carbonate (BBC) species, adsorbed on CHT-*x*, seems to be more favorable for the reaction than chelating bidentate carbonate (CBC) species.

Moreover, the used CHT-1 was washed several times with ethanol, dried and reused to explore the recyclability (results listed in Table 4). It can be found that the glycerol conversion decreases while the GC selectivity increases, which can be ascribed to the existence of zinc glycerolate on the surface of the used catalyst. In addition, the decrease of glycerol conversion may result from the loss of the active component (Zn^{2+}) by leaching.[29] The reaction solution (catalyst: CHT-1) was detected by ICP (Thermo iCAP 6300), and the result shows that the content of zinc ions in the reaction solution is about 0.59%.

Effect of introduction of Li, Mg and Zr on CHT-1 catalyst

It is well known that the acid–base properties of the catalysts can be modified by changing the cations in the layers; the compensating anions or activation method.[28] Therefore, in order to improve further the catalytic performance, the CHT-1 sample was modified by Li, Mg and Zr, and investigated for the synthesis of GC. The physical–chemical properties and their relationship with the catalytic performance were also studied.

Fig. 6a shows the XRD patterns of the precursors. Compared with HT-1, the crystallinity of the HTlcs decreases with the introduction of a fourth element (Li, Mg and Zr), especially for HT-Zr, probably due to the distortions of the HTl layers as a result of the replacement of Al^{3+} (ionic radius 0.053 nm) by Zr^{4+} (ionic radius 0.072 nm).[40] The lowest peak intensity of ZnO in HT-Li suggests the highest dispersion of ZnO. Furthermore, the strongest peak intensity of ZnO in HT-Mg can be ascribed to the high M^{2+}/M^{3+} ratio ($(Zn^{2+} + Mg^{2+})/Al^{3+} = 5$); previous reports suggested that an atomic ratio of M^{2+}/M^{3+} between 2 to 4 was favorable for the synthesis of HTlcs.[36]

Fig. 6b shows the XRD patterns of the calcined samples. It is observed that upon thermal decomposition at 500 °C, the HTl structure collapses and forms the corresponding metal oxide/carbonate. The sharp diffraction peaks of ZnO appearing on CHT-Mg suggest that the introduction of Mg leads to the aggregation of Zn atoms. The La prefers to locate

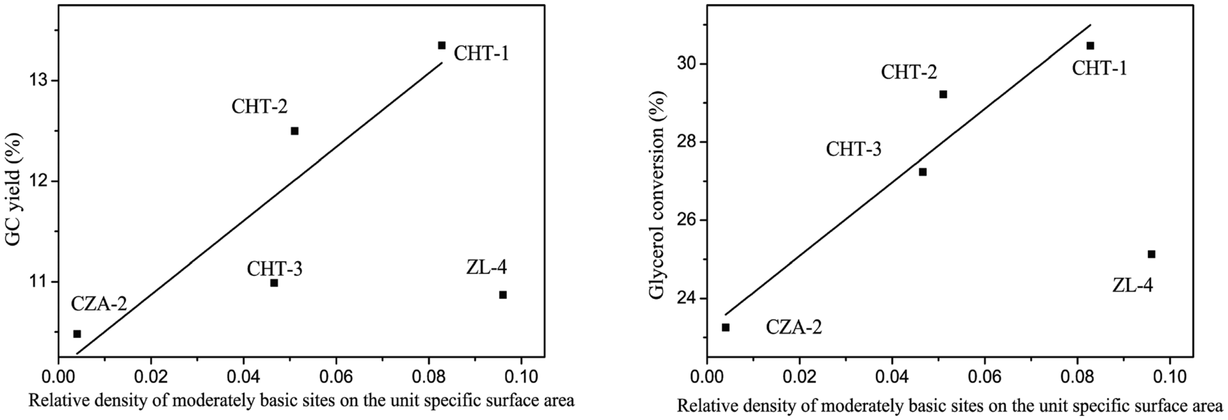

Fig. 5 The relationship between catalytic activity and density of moderately basic sites. The density of moderately basic sites can be obtained by division of the peak area value of moderately basic sites (Fig. 4) by the specific surface area (in Table 1), and the calculated results multiplied by 10^{10}.

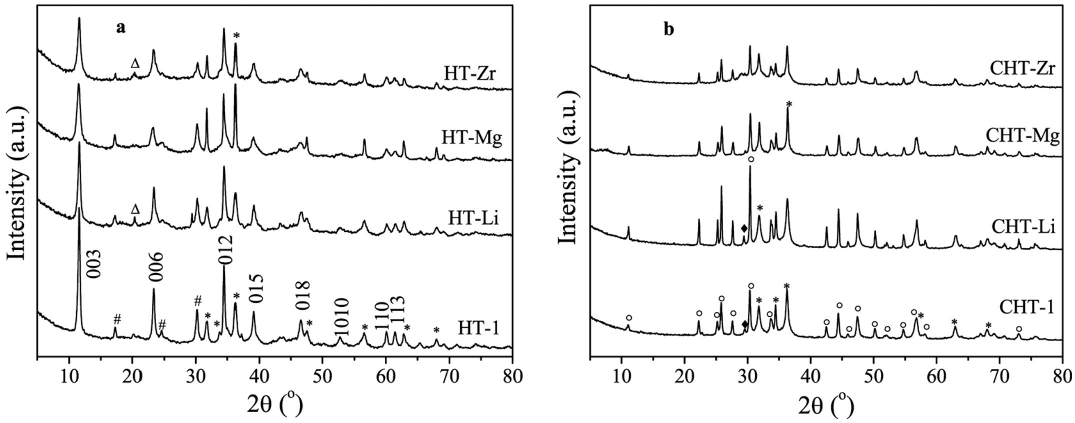

Fig. 6 (a) XRD patterns of HT-1 and HT-M samples. #: $LaCO_3OH$ (JCPDS 26-815); *: ZnO; Δ: $La_2(CO_3)_2(OH)_2$ (JCPDS 70-1774). (b) XRD patterns of calcined catalysts. ○: hexagonal $La_2O_2CO_3$ (JCPDS 37-804); ♦: monoclinic $La_2O_2CO_3$ (JCPDS 48-1113).

in the interlayer gallery of HT as separate hydroxide and hydroxyl carbonate phases.[38] The smallest value of the parameter *c* in HT-Li (Table 1) leads to the lowest interlayer La content which results in the strongest peak intensity of $La_2O_2CO_3$ appearing in CHT-Li. In the same way, the biggest value of the parameter *c* in HT-Zr leads to greater amounts of La located in the interlayer space and results in the lowest peak intensity of $La_2O_2CO_3$. Moreover, according to the results of TG analysis (Fig. S3†), Mg may exist in the form of $MgCO_3$ in the CHT-Mg.

The textures of the calcined samples are listed in Table 1. Compared with CHT-1, the specific surface area increases significantly from 36.4 to 82.5 $m^2\ g^{-1}$ with the introduction of Li and Mg, while it decreases to 26.4 $m^2\ g^{-1}$ for CHT-Zr. The pore volume and pore radius also increase with the introduction of Li, Mg and Zr. The increase of specific surface area, pore volume and pore radius for CHT-Li and CHT-Mg can be ascribed to the greater content of hydroxyl groups and carbonate anions with the introduction of cations (see Fig. S3,† the weight loss of the second stage), because more open, porous networks are produced after thermal treatment. In addition, the decrease of the specific surface area in CHT-Zr can be related to the introduction of Zr which is not favorable for the synthesis of hydrotalcites,[40] as described in XRD results.

The calcined samples were analyzed by XPS, and the binding energies (BE) of $Zn2p_{3/2}$, Al2p and La3d are presented in Table 3. For all samples, peaks are found at around 834.4–834.8 eV (BE) for La3d. The $Zn2p_{3/2}$ peak at 1020.8–1021.6 eV can be assigned to the Zn^{2+} species on the catalyst surface. It can be seen that the BE of $Zn2p_{3/2}$ and La3d increase with the introduction of Li, Mg and Zr while the BE of Al decreases. The results reveal that the interactions between ZnO, $La_2O_2CO_3$ and Al_2O_3 changed with the introduction of Li^+, Mg^{2+} and Zr^{4+}. Compared with CHT, the BE of Zn increases with the introduction of Li, Mg and Zr, especially for CHT-Li and CHT-Zr. For CHT-Li, the high BE of $Zn2p_{3/2}$ can be ascribed to electron transfer from Zn atoms to Li acceptors,[55,56] while the high BE of $Zn2p_{3/2}$ in CHT-Zr might be attributed to electron transfer from Zn atoms to Zr atoms or oxygen atoms. The high BE of $Zn2p_{3/2}$ in CHT-Li and CHT-Zr is favorable for the activation of glycerol.[49]

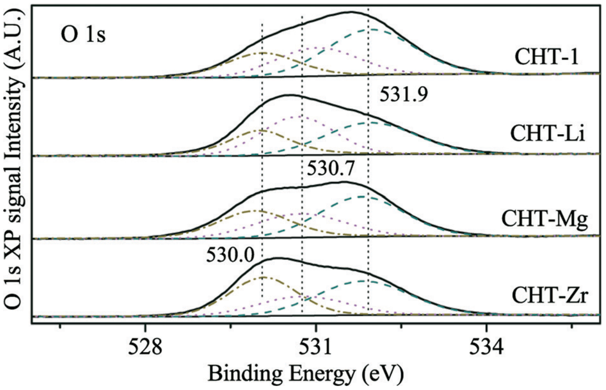

Fig. 7 O 1s XP spectra for CHT-1 and CHT-M catalysts.

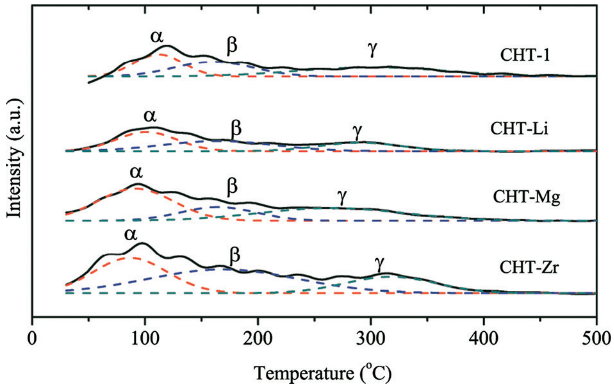

Fig. 8 CO_2-TPD profiles of the prepared catalysts. The values of peak (β and γ) area of CHT-1, CHT-Li, CHT-Mg and CHT-Zr were multiplied by 10^{10} and the results are 3.019, 2.431, 3.837 and 6.613 (a.u.) g^{-1}, respectively.

Surface compositions of the catalysts, as determined by XPS, are also shown in Table 3. It is found that the surface content of Zn^{2+} in CHT-Li is higher than in CHT, suggesting that the introduction of Li favors the enrichment of Zn atoms on the surface of the catalysts. For CHT-Mg, the introduction of Mg decreases the surface content of Zn atoms. In addition, the high surface content of Li in CHT-Li favors the enhancement of the interaction with surface Zn atoms, and then results in the increase of the BE of $Zn2p_{3/2}$ in CHT-Li.

Fig. 7 shows the O 1s XPS results over CHT and CHT-M catalysts. The peak can be deconvoluted into three peaks, which are referred to the oxygen ions in the crystal lattice (~530.0 eV), adsorbed oxygen species (~530.7 eV), as well as hydroxyl and carbonate species (~531.9 eV).[57] The quantification of each surface oxygen species was calculated and shown in Table 5. It can be seen that the amount of lattice oxygen species increases with the introduction of Li, Mg and Zr. For metal oxides, the lattice oxygen on the surface is considered to act as Lewis basic sites.[58] Therefore, the increase of the amount of lattice oxygen may increases the amount of basic sites and thus favors CO_2 adsorption and activation. In addition, due to the imbalance of oxidation state between Li($^{+}$) and Zn($^{2+}$) site, oxygen vacancies are created in CHT-Li, resulting in the increase of the amount of surface adsorption oxygen species (O^{2-} and O^{-}/O^{2-}).[57]

The basicity of the catalysts was measured by CO_2-TPD (Fig. 8). All profiles can be deconvoluted into three Gaussian peaks assigned to weakly (α peak) and moderately (β and γ peak) basic sites, and the values of the peak area can be considered to the relative amount of basic sites. The increase of peak area in CHT-Mg and CHT-Zr suggests the increase of the amount of weakly basic sites with the introduction of Mg and Zr. Compared with CHT, the values of peak area of β and γ decrease for CHT-Li, while they increase for CHT-Mg and CHT-Zr which can be explained as follows:

Previous reports described that the number of lattice oxygens was related to the Lewis basic sites for metal oxides.[58] For CHT-Li, the decrease of the amount of moderately basic sites can be ascribed to the high surface content of Li (+) which results in the decrease of the amount of surface lattice oxygen. The highest specific surface area and the introduction of alkaline earth metal oxides did not significantly improve the surface basicity for CHT-Mg. The TG analysis (Fig. S3†) suggests that $MgCO_3$ is formed during the decomposition process of hydrotalcites at 500 °C and then decomposed at around 536 °C. Therefore, the formation of $MgCO_3$ might be responsible for the reduced improvement of moderately basic sites. For CHT-Zr, the obvious increase of moderately basic sites can be attributed to the increase in the amount of surface lattice oxygen with the introduction of Zr (4+).

The catalytic performances of the Li, Mg and Zr modified catalysts are summarized in Table 4. Compared with CHT-1, the catalytic activity improves with the introduction of Li, Mg and Zr, especially for CHT-Li. A maximum GC yield of 15.1% with a glycerol conversion of 35.7% is obtained over CHT-Li. For comparison, the catalytic activities of Li_2CO_3, MgO and ZrO_2 were also studied (Table 4). It can be found that MgO

Table 5 Amount of each surface oxygen species on CHT-1 and CHT-M catalysts

	Amount of oxygen species[a]					
	Lattice oxygen		Adsorbed oxygen		Hydroxyl/carbonate	
Catalysts	%	BE/eV	%	BE/eV	%	BE/eV
CHT-1	31.6	530.1	32.5	531.0	35.8	532.0
CHT-Li	32.0	530.0	33.9	530.7	34.1	532.0
CHT-Mg	32.5	529.9	32.3	530.7	35.1	531.8
CHT-Zr	33.8	530.0	31.6	530.8	34.6	531.9

[a] Measured by XPS

and ZrO_2 are inactive toward the reaction, while Li_2CO_3 shows low activity for the synthesis of glycerol carbonate. The results suggest that the improvement of the catalytic activities for CHT-M can't be ascribed simply to the introduction of Li_2CO_3, MgO and ZrO_2. The improvement of the catalytic activities with the introduction of Li, Mg and Zr can be estimated from the catalyst characteristics.

In association with the results of N_2 adsorption, the introduction of Li and Mg improves the specific surface area which favors the exposure of more active sites, and then improves the catalytic activities. Despite the smallest surface area of CHT-Zr, the improvement of the catalytic activity suggests that this property is not just correlated to the surface area of the catalysts. Considering the XPS results, the increase of the BE of $Zn2p_{3/2}$ in CHT-M, especially in CHT-Li and CHT-Zr, favors the activation of glycerol.[49] In addition, the increase of the surface Zn content in CHT-Li is also helpful to improve the glycerol activation. Furthermore, according to the results of CO_2-TPD, the amount of moderately basic sites increases for CHT-Mg and CHT-Zr. Because of the smallest surface area of CHT-Zr, the improvement of the catalytic activity can be associated with the large amount of moderately basic sites, which favors CO_2 adsorption and activation. However, the best catalytic performance and smallest amount of moderately basic sites of CHT-Li indicate that the amount of moderately basic sites is not the key factor for catalytic activity. As described by previous reports,[49] the catalytic activity relates to the surface area, the BE of Zn atoms, and the amount of moderately basic sites. In this case, the best catalytic activity for CHT-Li may result from the high binding energy of Zn $2p_{3/2}$ as well as the high surface Zn content. Moreover, the improvement of catalytic activity for CHT-Li may be also related to the activity of Li_2CO_3 itself. The lower catalytic activities of CHT-Mg and CHT-Zr may be attributed to the low surface Zn content (Table 3) and small surface area (Table 1), respectively.

Effect of reaction conditions

CHT-Li was chosen as a typical catalyst to investigate the effect of the reaction conditions on the catalytic activity. It has been stated that CH_3CN is very important for the reaction. Therefore, the effect of the amounts of CH_3CN on the yield of GC was investigated in detail. As shown in Fig. 9a, the glycerol conversion and GC yield increase remarkably with the increase of the CH_3CN amount from 3 to 7 mL, and when the amount of CH_3CN increases form 7 mL to 11 mL the conversion of glycerol does not increase significantly. As described in previous reports,[22,24] CO_2 was easily dissolved in CH_3CN, and the CO_2 concentration in the liquid increases with the increase of the amount of CH_3CN, which leads to higher catalytic activity. In addition, CH_3CN can shift the equilibrium of the reaction, which improves the catalytic activity by removing the formed H_2O.

Fig. 9b shows the effect of catalyst amount on the reaction. The results demonstrate clearly that GC selectivity and GC yield increase with the increase of catalyst amount from 1 to 3 wt% of glycerol and decrease with the further increase of catalyst amount, especially for GC selectivity. The glycerol conversion increases with the increase of catalyst amount. The dropping of the GC selectivity may be ascribed to the enhancement of acetonitrile hydrolysis with the increase of catalyst amount. Greater amounts of catalyst favor the hydrolysis of acetonitrile and then produce higher amounts of acetic acid, which results in the formation of more byproduct.

As shown in Fig. 9c, the conversion of glycerol and GC yield increase with the increase of reaction temperature in the range of 150–170 °C. But further increase of temperature leads to the decrease of the GC yield which can be ascribed to the remarkable decrease of GC selectivity. A previous report[16] described that the decomposition or transformation of glycerol carbonate could occur at high temperature or in the presence of amino groups (*e.g.* acetamide in our experiment). Therefore, the higher temperature leads to lower catalytic activity. A suitable reaction temperature for the reaction should be about 170 °C.

Fig. 9d shows the effect of reaction time on the reaction. The conversion of glycerol and GC yield increase rapidly within the first 12 h, and then change little afterwards, indicating the approach of thermodynamic equilibrium. The glycerol conversion and GC yield are not obviously improved after 14 h. Thus, 14 h is the optimal reaction time for the reaction.

As described by previous reports,[22,59] increasing the CO_2 pressure improves the conversion of glycerol, GC yield and GC selectivity (Fig. 9e). In our experiment, a high CO_2 pressure is favorable for achieving high GC yield, which could be ascribed to the increase in CO_2 dissolved in CH_3CN with the increase of CO_2 pressure; a high CO_2 concentration in the liquid could promote the conversion of glycerol. With the increase of the pressure in the range 2.0–6.0 MPa, the conversion of glycerol increases from 27.3% to 39.5%, and the yield of GC increases from 11.5% to 18.7%.

The possible mechanisms of glycerol carbonate synthesis

In order to understand the reaction mechanism, the CO_2 adsorption species were performed by DRIFTS and the spectra of CO_2 adsorbed on mixed oxides are shown in Fig. 10. The CO_2 adsorption modes identified in previous work are shown in Scheme 1.[60–62] The formation of different species might stem from different basic sites: *e.g.* monodentate (unidentate) carbonate (MC), adsorbed on oxygen ions with the lowest coordination number, can be attributed to strongly basic sites. Bridged bidentate carbonate (BBC) and chelating bidentate carbonate (CBC) adsorbed on M^{n+}–O^{2-} pairs can be assigned to moderately basic sites.[61] Moreover, the weakly basic sites may be associated with the surface hydroxyl groups (OH^-) over which the CO_2 adsorption species is present in the form of bicarbonate.

For CZA-2, the spectra show four main peaks at around 1701, 1657, 1272 and 1228 cm^{-1}. The peaks at 1657 and 1272 cm^{-1}

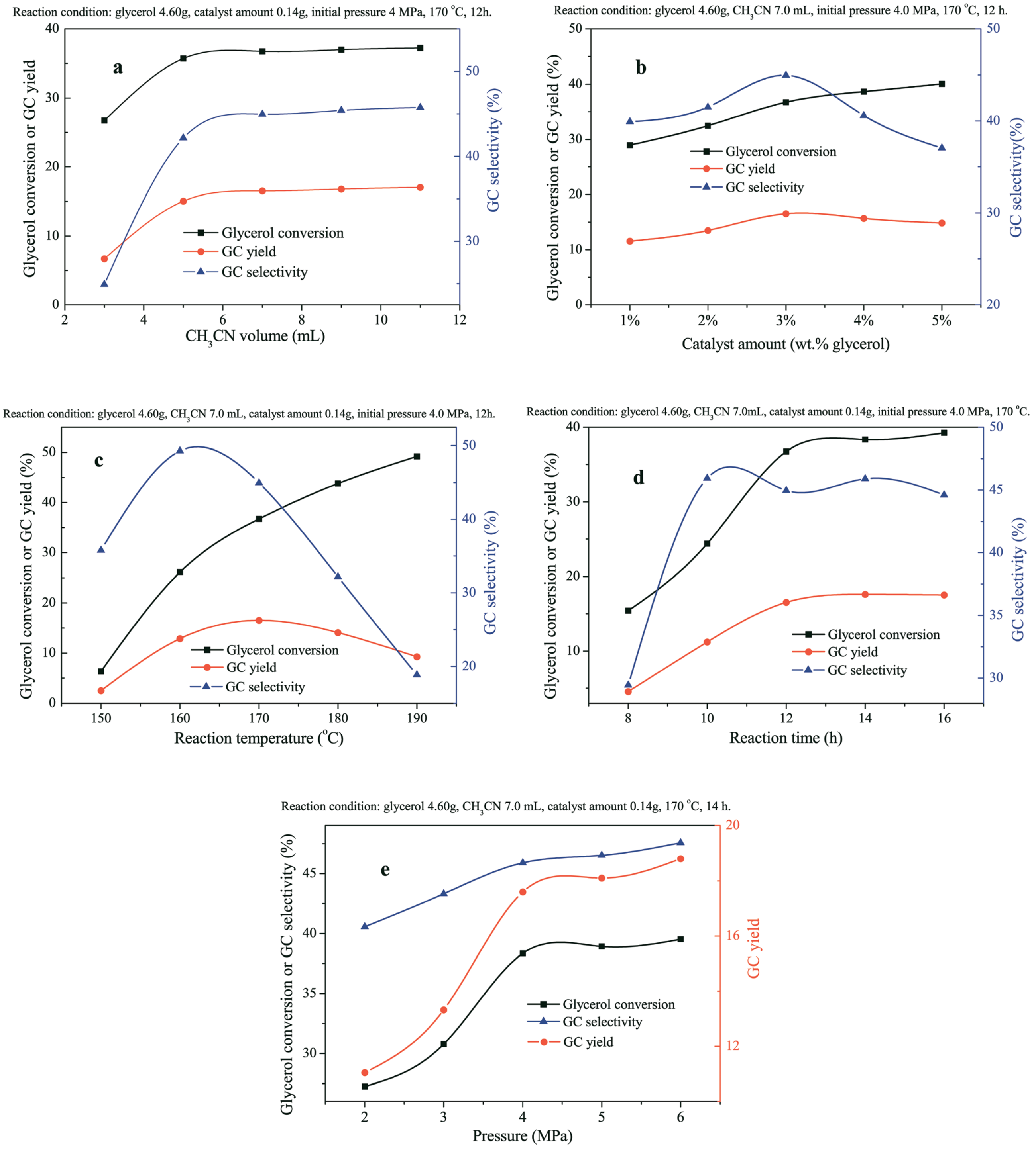
Reaction condition: glycerol 4.60g, catalyst amount 0.14g, initial pressure 4 MPa, 170 °C, 12h.

Reaction condition: glycerol 4.60g, CH_3CN 7.0 mL, initial pressure 4.0 MPa, 170 °C, 12 h.

Reaction condition: glycerol 4.60g, CH_3CN 7.0 mL, catalyst amount 0.14g, initial pressure 4.0 MPa, 12h.

Reaction condition: glycerol 4.60g, CH_3CN 7.0mL, catalyst amount 0.14g, initial pressure 4.0 MPa, 170 °C.

Reaction condition: glycerol 4.60g, CH_3CN 7.0 mL, catalyst amount 0.14g, 170 °C, 14 h.

Fig. 9 Effect of reaction conditions (a: CH_3CN amount, b: reaction temperature, c: catalyst amount, d: reaction time, e: CO_2 pressure) on the catalytic activity.

are assigned to BBC species,[60] while 1701 and 1228 cm^{-1} are associated with the CBC species adsorbed on Al_2O_3,[62] as well as the ν_{as}(C–O) mode of HCO_3^- (bicarbonate species),[63] respectively. Most of the adsorbed CO_2 species desorbed after sweeping with Ar for 5 min which indicates the surface of CZA-2 was dominated by weakly basic sites. For CZL-4, the band at 1587 cm^{-1} can be ascribed to the CBC species, while 1309 cm^{-1} can be assigned to the MC species. In addition, the band at 1201 cm^{-1} is characteristic for BBC species.[62] Even after purging by Ar for 30 min, the adsorption peaks still exist which indicates that the introduction of La improved the basicity of the catalyst, especially for moderately basic sites. For CHT-*x* catalysts, the formation of BBC bands at 1621–1651 cm^{-1}, MC bands at 1302–1321 cm^{-1} and

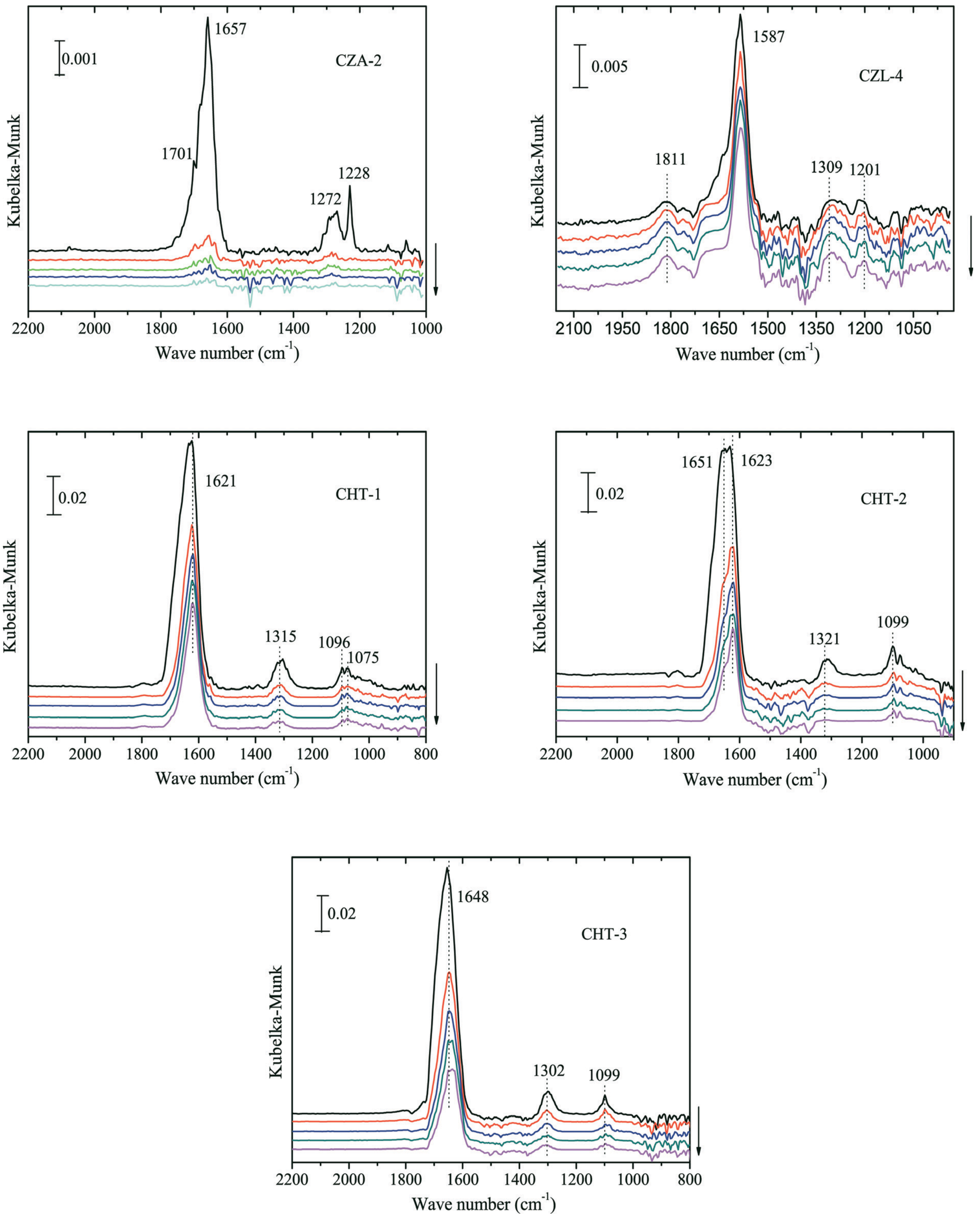

Fig. 10 DRIFTS spectra of CO_2 adsorbed on the catalysts at 170 °C after the purging gas was switched to Ar from CO_2 for 0.0, 5.0 10.0 20.0 and 30.0 min.

1020 cm^{-1}, and free carbonate bands at 1075, 1096 and 1099 cm^{-1} (ref. 62, 64) can be observed. BBC is the main species upon CO_2 adsorption at 170 °C.

Compared with CZA-2, greater amounts of CBC are formed on the surface of CZL-4, which may be ascribed to the formation of $La_2O_2CO_3$. In addition, the introduction of Al leads to the BBC species becoming the main adsorption pattern. A previous report indicated that CBC is more stable than BBC.[65] The transformation of the CO_2 adsorption species from CBC to BBC may results in a shift of the desorption

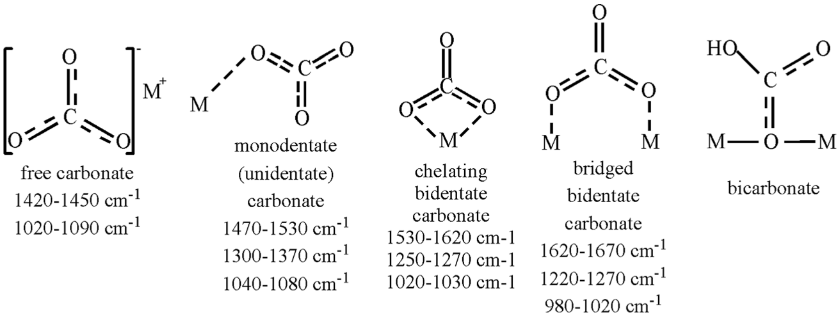

Scheme 1 Species of CO_2 adsorption.

temperature to lower temperatures, which is in accordance with the CO_2-TPD results (Fig. 4). Moreover, it can be seen that CHT-*x* catalysts have a strong peak intensity, indicating that CHT-*x* catalysts have greater amounts of moderately basic sites than CZL-4 which may be associated with the larger surface area of the CHT-*x* catalysts.

The used catalysts are isolated and characterized by FT-IR to gain a clear understanding of the nature of the active species for the reaction (Fig. 11). The band at 1950 cm^{-1} is assigned to the O–H⋯O bending mode of zinc glycerolate ($Zn(C_3H_6O_3)$) formed from the reaction of glycerol and ZnO.[31] With the formation of zinc glycerolate, a new C–H stretching band at 2842 cm^{-1} is also observed and the C–O stretching of glycerol at 1046 and 1111 cm^{-1} shifts to higher frequencies. The strong absorption band of zinc glycerolate on CZL-4 may be associated with the high surface Zn content and the high valence state of Zn atoms (Table 3) which favors the activation of glycerol.[29,49] In addition, the intensity of bands at 1950 cm^{-1} decreases with the increase of Al content in CHT-*x* catalysts, suggesting a decrease in the amount of zinc glycerolate, which also explained the decrease of catalytic activity upon increasing Al content for CHT-*x* catalysts.

Previous reports[19,20,66] suggest that cyclic carbonate was formed through the insertion of activated CO_2 to metal alkoxides followed by intramolecular nucleophilic attack of alkoxy groups to carbonyl carbon atoms. In our experiment, the results of DRIFTS spectra of CO_2 activation suggest that the bridged bidentate carbonate was the main adsorption mode at 170 °C (reaction temperature) on CHT-*x* catalysts. Therefore, the activated CO_2 may be in the form of a bridged bidentate carbonate that inserts into the zinc glycerolate to form a cyclic metal carbonate (A in Scheme 2) followed by intramolecular rearrangement to produce glycerol carbonate.

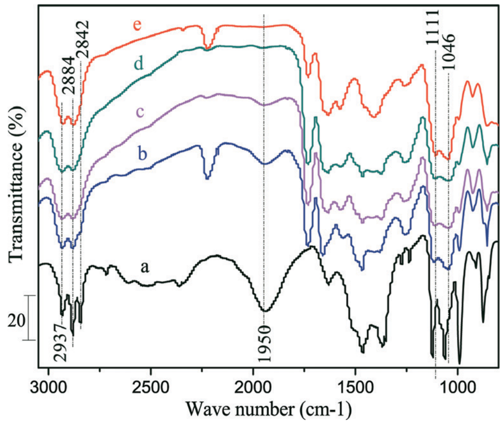

Fig. 11 The FT-IR spectra of the used catalysts. (a) CZL-4 used (b) CHT-1 used, (c) CHT-2 used, (d) CHT-3 used, (e) CZA-2 used.

Although similar intermediate species of seven-membered ring esters (A species) have been proposed by many researchers,[16,17,64] direct evidence has not been presented to date. Therefore, in order to confirm or verify the above hypothesis, zinc glycerolate is prepared (Fig. S4 and S5†) and the reaction of zinc glycerolate and CO_2 is studied by DRIFTS (Fig. 12). It is found that with the increasing of reaction temperature, new bands at 1778, 1462, 1124, 1061, 1043 and 994 cm^{-1} are observed. In addition, the bands between 900 and 1300 cm^{-1} can be ascribed to the stretching vibration of C–O or C–O–C. It has been reported[67] that five-membered ring esters have C=O frequencies somewhat higher than those in seven-membered ring esters because of the high ring-strain in five-membered ring esters. Therefore, the new band at 1778 cm^{-1} may be ascribed to the C=O stretching mode in the seven-membered ring ester (A in Scheme 2), which shifts to 1787 cm^{-1} for glycerol carbonate. The above analysis suggests that seven-membered ring esters may be stable.

Theoretical calculation methods are performed to verify the stability of the A species (Fig. 13). The calculation results show that optimized structures are stable and reliable. The A species was formed through the insertion of activated CO_2 to zinc glycerolate. Compared with CO_2, the distances of C1–O2 and C1–O3 increase from 1.180 Å (in the free CO_2) to 1.206 and 1.323 Å, respectively, because of the steric effect in the A species. The distance of a newly formed Zn–O3 bond in the A species is 1.898 Å, while the distance of newly formed C1–O1 is 1.471 Å. The calculated results suggest that the A species is stable, which is in accordance with the DRIFTS results. Furthermore, compared with Zn–O4, the longer bond distances of Zn–O3 tend to break down which may result in the formation of ZnO (Zn–O4) and glycerol carbonate through the attack of C3 by the lone pair electrons of O3, accompanied by the breaking of the band of C3–O4.

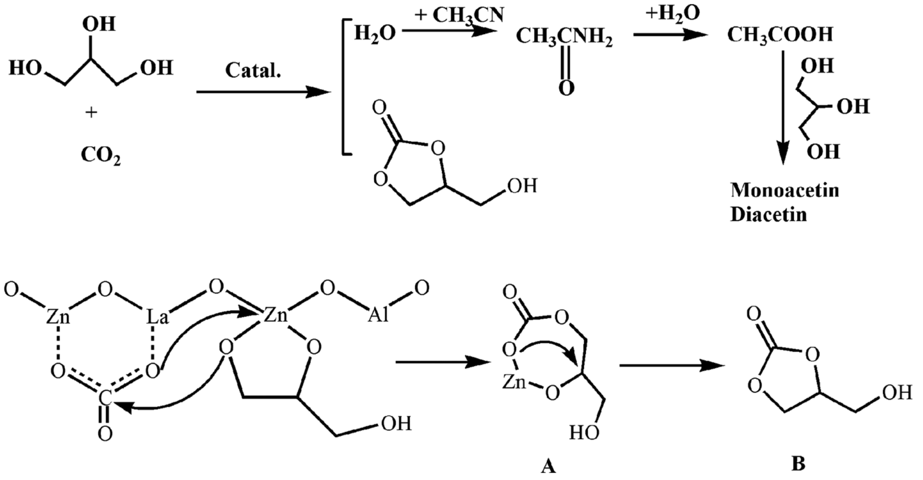

Scheme 2 The reaction roadmap and the mechanism of insertion of activated CO_2 to zinc glycerolate to form glycerol carbonate.

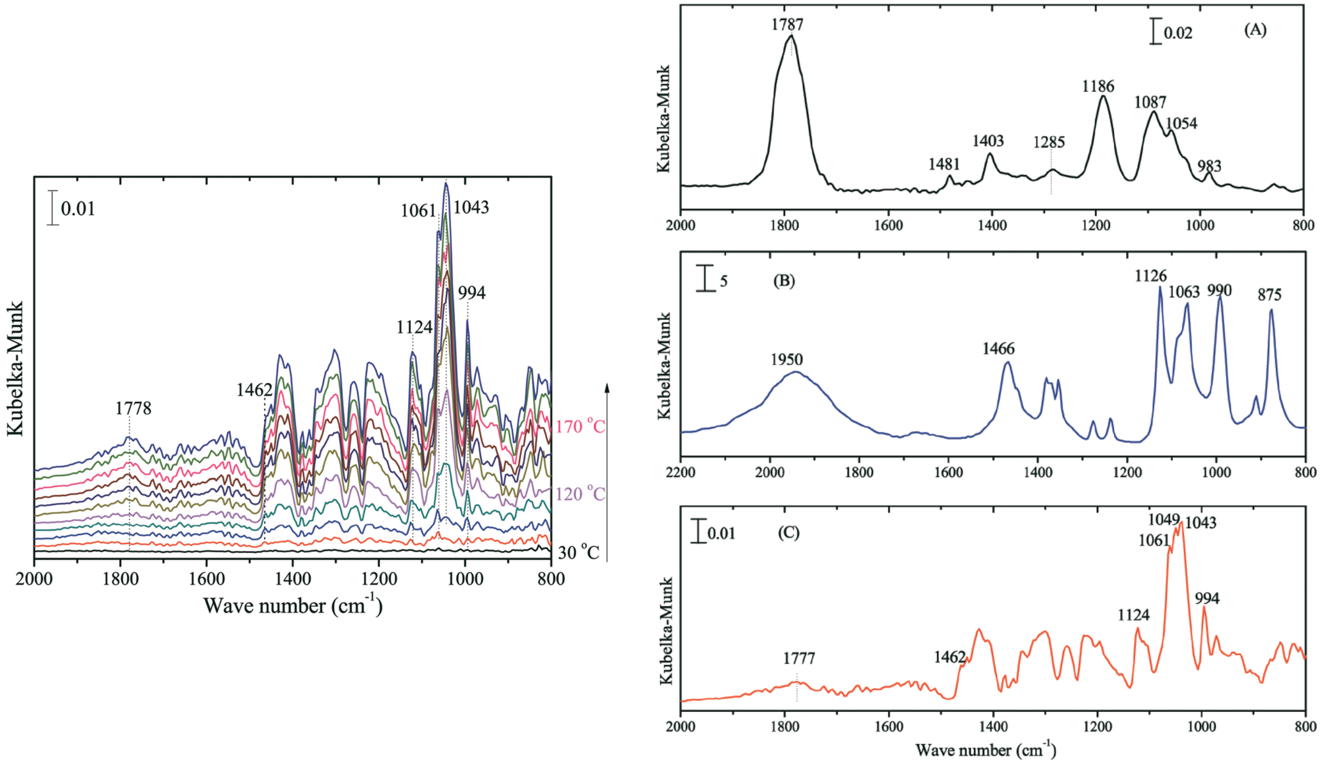

Fig. 12 DRIFTS spectra of the zinc glycerolate reaction with CO_2 at the temperatures of 30, 60, 80, 100, 120, 140, 150, 160, 170, 180 and 190 °C, and the spectra of glycerol carbonate (A), zinc glycerolate (B) and the reacted spectra at 170 °C of zinc glycerolate with CO_2 (C).

Moreover, the Gibbs free energies of the formation of A and glycerol carbonate are calculated (under ideal conditions) and the results are shown in Table 6. The $\Delta_r G$ of the formation of A is negative while the $\Delta_r G$ of the transformation of A species to glycerol carbonate is 67.32 kcal mol^{-1} which means that the intra-molecular rearrangement step may be the rate-determining step. In fact, the reaction was performed under high temperature and high pressure which will decrease the Gibbs free energy of the reaction. Previous reports showed that it is very easy for Zn^{2+} to form complexes with O and N atoms.[29,68] In our study, the N and O atoms in acetamide and acetic acid produced by the hydrolysis of acetonitrile may form complexes with Zn atom (in A species), as described by Fujita *et al.*,[29] which may be beneficial for the removal of ZnO and reduce the Gibbs free energy of the intra-molecular rearrangement stage, which then favors the formation of glycerol carbonate.

The results of DRIFTS of zinc glycerolate reaction with CO_2 and theoretical calculations indicate that the proposed reaction mechanism is reasonable, that the A species produced by the insertion of activated CO_2 to zinc glycerolate is stable and that the process happens spontaneously. The

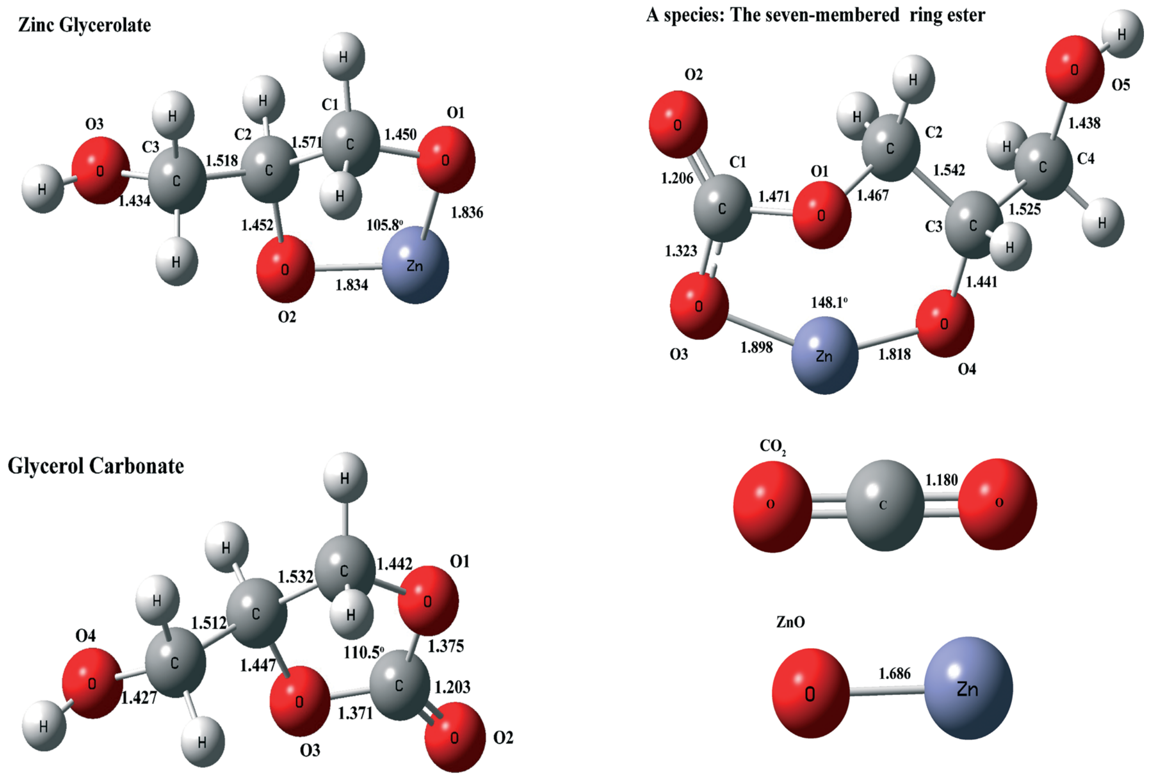

Fig. 13 The optimized geometries of zinc glycerolate, A species and glycerol carbonate. The bond distances (in angstroms) and angles (in degrees) are labeled in the corresponding positions.

Table 6 The calculated Δ_rG of the formation of A species and glycerol carbonate

Reaction equation	Δ_rG^a/kcal mol^{-1}
Zinc glycerolate + CO_2 → A species	−7.75
A species → glycerol carbonate + ZnO	67.32

[a] The values are the theoretical calculation results.

process of glycerol carbonate formation by the intramolecular rearrangement of the A species is the rate-determining step.

4. Conclusions

The Zn/La/Al and Zn/Al/La/M (M = Li, Mg, Zr) catalysts derived from hydrotalcite-like compounds were synthesized by a co-precipitation method. The introduction of La and the Al content have a significant influence on the physicochemical and catalytic properties of the Zn/La/Al catalysts for glycerol carbonate synthesized from glycerol carbonylation with CO_2. For Zn/Al/La/M catalysts, the introduction of Li, Mg and Zr improved obviously the catalytic activities. Moreover, DRIFTS and theoretical calculations were used to explore the reaction mechanism. The following conclusions may be drawn:

(1) The pure and crystalline Zn/La/Al hydrotalcite-like compounds can be formed by the replacement of Al^{3+} with La^{3+}, and the yields of the hydrotalcite-like phase reach a maximum at $Zn^{2+}/La^{3+}/Al^{3+} = 4:1:2$.

(2) With the increase of Al content, the specific surface area increases, while the surface zinc content, the binding energy of the zinc atom and the density of the moderately basic sites decrease. Moreover, compared with the Zn/Al hydrotalcite structure, the thermal stability of the Zn/La/Al hydrotalcite-like structure decreases.

(3) For Li, Mg and Zr modified Zn/Al/La catalysts, the specific surface area increases with the introduction of Li and Mg while it decreases for Zr. The binding energy of Zn $2p_{3/2}$ increases with the introduction of Li, Mg and Zr. Moreover, the catalysts' basicity is improved by the introduction Mg and Zr.

(4) For Zn/Al/La catalysts, good catalytic performance is obtained on Zn/La/Al = 4 : 1 : 1. In addition, the catalytic activities are improved obviously with the Li, Mg and Zr modified Zn/Al/La catalysts. It is found that the good catalytic activity may be associated with the large specific surface area, the high surface content of Zn and the high binding energy of Zn atoms, as well as high density of moderately basic sites.

(5) Under optimal reaction conditions (CH_3CN 7.0 mL, catalyst amount 0.14 g, 170 °C, 14 h, P_{CO_2} = 6.0 MPa), the conversion of glycerol and the yield of glycerol carbonate are 39.5% and 18.7%.

(6) The activated CO_2 should be inserted zinc glycerolate in the form of bidentate carbonate to form a seven-

membered ring ester followed by intramolecular rearrangement to form glycerol carbonate.

(7) The theoretical calculation results verified that the seven-membered ring ester is stable and the formation process happens spontaneously. The intramolecular rearrangement of the seven-membered ring ester to form glycerol carbonate is the rate-determining stage.

Acknowledgements

This work was financially supported by the National Natural Science Foundation of China (21306217) and "Strategic Priority Research Program – Climate Change, and Carbon Budget and Related Issues" of the Chinese Academy of Sciences, grants no. XDA05010109, XDA05010110, XDA05010204.

Notes and references

1 P. R. Muniyappa, S. C. Brammer and H. Noureddini, *Bioresour. Technol.*, 1996, **56**, 19–24.

2 C. H. Zhou, J. N. Beltramini, Y. X. Fan and G. Q. Lu, *Chem. Soc. Rev.*, 2008, **37**, 527–549.

3 A. E. Diaz-Alvarez, J. Francos, B. Lastra-Barreira, P. Crochet and V. Cadierno, *Chem. Commun.*, 2011, **47**, 6208–6227.

4 A. Behr, J. Eilting, K. Irawadi, J. Leschinski and F. Lindner, *Green Chem.*, 2008, **10**, 13.

5 Mario Pagliaro and Michele Rossi, *The Future of Glycerol: New Usages for a Versatile Raw Material*, RSC Publishing, Cambridge, 2008.

6 M. Pagliaro, R. Ciriminna, H. Kimura, M. Rossi and C. Della Pina, *Angew. Chem., Int. Ed.*, 2007, **46**, 4434–4440.

7 J. R. Ochoa-Gómez, O. Gómez-Jiménez-Aberasturi, B. Maestro-Madurga, A. Pesquera-Rodríguez, C. Ramírez-López, L. Lorenzo-Ibarreta, J. Torrecilla-Soria and M. C. Villarán-Velasco, *Appl. Catal., A*, 2009, **366**, 315–324.

8 A. Takagaki, K. Iwatani, S. Nishimura and K. Ebitani, *Green Chem.*, 2010, **12**, 578–581.

9 M. J. Climent, A. Corma, P. De Frutos, S. Iborra, M. Noy, A. Velty and P. Concepción, *J. Catal.*, 2010, **269**, 140–149.

10 M. Malyaadri, K. Jagadeeswaraiah, P. S. Sai Prasad and N. Lingaiah, *Appl. Catal., A*, 2011, **401**, 153–157.

11 F. S. H. Simanjuntak, T. K. Kim, S. D. Lee, B. S. Ahn, H. S. Kim and H. Lee, *Appl. Catal., A*, 2011, **401**, 220–225.

12 M. G. Álvarez, M. Plíšková, A. M. Segarra, F. Medina and F. Figueras, *Appl. Catal., B*, 2012, **113–114**, 212–220.

13 A. Kumar, K. Iwatani, S. Nishimura, A. Takagaki and K. Ebitani, *Catal. Today*, 2012, **185**, 241–246.

14 M. Aresta, A. Dibenedetto, F. Nocito and C. Ferragina, *J. Catal.*, 2009, **268**, 106–114.

15 F. Rubio-Marcos, V. Calvino-Casilda, M. A. Bañares and J. F. Fernandez, *J. Catal.*, 2010, **275**, 288–293.

16 C. Hammond, J. A. Lopez-Sanchez, M. H. A. Rahim, N. Dimitratos, R. L. Jenkins, A. F. Carley, Q. He, C. J. Kiely, D. W. Knighta and G. J. Hutchings, *Dalton Trans.*, 2011, **40**, 3927–3937.

17 J. Li and T. Wang, *Chem. Eng. Process.*, 2010, **49**, 530–535.

18 C. Vieville, J. W. Yoo, S. Pelet and Z. Mouloungui, *Catal. Lett.*, 1998, **56**, 245–247.

19 M. Aresta, A. Dibenedetto, F. Nocito and C. Pastore, *J. Mol. Catal. A: Chem.*, 2006, **257**, 149–153.

20 J. George, Y. Patel, S. M. Pillai and P. Munshi, *J. Mol. Catal. A: Chem.*, 2009, **304**, 1–7.

21 A. Dibenedetto, A. Angelini, M. Aresta, J. Ethiraj, C. Fragale and F. Nocito, *Tetrahedron*, 2011, **67**, 1308–1313.

22 S. Huang, J. Ma, J. Li, N. Zhao, W. Wei and Y. Sun, *Catal. Commun.*, 2008, **9**, 276–280.

23 H. Chen, X. Zhao and Y. Wang, *Gaoxiao Huaxue Gongcheng Xuebao*, 2006, **20**, 734–739.

24 K. Tomishige, H. Yasuda, Y. Yoshida, M. Nurunnabi, B. Li and K. Kunimori, *Green Chem.*, 2004, **6**, 206–214.

25 L. H. Zhang, C. Zheng, F. Li, D. G. Evans and X. Duan, *J. Mater. Sci.*, 2008, **43**, 237–243.

26 F. M. A. Alejandre, P. Salagre, X. Correig and J. E. Sueiras, *Chem. Mater.*, 1999, **11**, 939–948.

27 G. Busca, U. Costantino, F. Marmottini, T. Montanari, P. Patrono, F. Pinzari and G. Ramis, *Appl. Catal., A*, 2006, **310**, 70–78.

28 F. Prinetto and G. Ghiotti, *J. Phys. Chem. B*, 2000, **104**, 11117–11126.

29 S. Fujita, Y. Yamanishi and M. Arai, *J. Catal.*, 2013, **297**, 137–141.

30 Z. M. S. Claude, J.-W. Yoo and A. Gaset, *US Pat.* 6025504, 2000.

31 J.-H. Park, J. S. Choi, S. K. Woo, S. D. Lee, M. Cheong, H. S. Kim and H. Lee, *Appl. Catal., A*, 2012, **433–434**, 35–40.

32 A. Serrano-Lotina, A. J. Martin, M. A. Folgado and L. Daza, *Int. J. Hydrogen Energy*, 2012, **37**, 12342–12350.

33 M. A. Bos and A. J. Koplick, *WO Pat.* WO 94/10113, 1994.

34 M. J. Frisch, *GAUSSIAN 09 (Revision A.02)*, Gaussian, Inc., Wallingford, CT, 2009.

35 J. T. Kloprogge, L. Hickey and R. L. Frost, *J. Solid State Chem.*, 2004, **177**, 4047–4057.

36 M. G. Álvarez, R. J. Chimentão, F. Figueras and F. Medina, *Appl. Clay Sci.*, 2012, **58**, 16–24.

37 P. Benito, I. Guinea, F. M. Labajos, J. Rocha and V. Rives, *Microporous Mesoporous Mater.*, 2008, **110**, 292–302.

38 P. Unnikrishnan and D. Srinivas, *Ind. Eng. Chem. Res.*, 2012, **51**, 6356–6363.

39 E. Rodrigues, P. Pereira, T. Martins, F. Vargas, T. Scheller, J. Correa, J. Del Nero, S. G. C. Moreira, W. Ertel-Ingrisch, C. P. De Campos and A. Gigler, *Mater. Lett.*, 2012, **78**, 195–198.

40 P. Gao, F. Li, H. Zhan, N. Zhao, F. Xiao, W. Wei, L. Zhong, H. Wang and Y. Sun, *J. Catal.*, 2013, **298**, 51–60.

41 H. Prescott, Z. Li, E. Kemnitz, A. Trunschke, J. Deutsch, H. Lieske and A. Auroux, *J. Catal.*, 2005, **234**, 119–130.

42 L. C. Meher, R. Gopinath, S. N. Naik and A. K. Dalai, *Ind. Eng. Chem. Res.*, 2009, **48**, 1840–1846.

43 D. G. Cantrell, L. J. Gillie, A. F. Lee and K. Wilson, *Appl. Catal., A*, 2005, **287**, 183–190.

44 Q. Mu and Y. Wang, *J. Alloys Compd.*, 2011, **509**, 396–401.

45 L. Jin, Y. Zhang, J. P. Dombrowski, C. Chen, A. Pravatas, L. Xu, C. Perkins and S. L. Suib, *Appl. Catal., B*, 2011, **103**, 200–205.

46 J. Sloczynski, R. Grabowski, P. Olszewski, A. Kozlowska, J. Stoch, M. Lachowska and J. Skrzypek, *Appl. Catal., A*, 2006, **310**, 127–137.

47 M. G. Alvarez, A. M. Segarra, S. Contreras, J. E. Sueiras, F. Medina and F. Figueras, *Chem. Eng. J.*, 2010, **161**, 340–345.

48 L. Wang, Y. Ma, Y. Wang, S. Liu and Y. Deng, *Catal. Commun.*, 2011, **12**, 1458–1462.

49 H. Li, D. Gao, P. Gao, F. Wang, N. Zhao, F. Xiao, W. Wei and Y. Sun, *Catal. Sci. Technol.*, 2013, **3**, 2801–2809.

50 G. Wu, X. Wang, W. Wei and Y. Sun, *Appl. Catal., A*, 2010, **377**, 107–113.

51 M. Rezayat and H. S. Ghaziaskar, *Green Chem.*, 2009, **11**, 710–715.

52 I. Dosuna-Rodríguez and E. M. Gaigneaux, *Catal. Today*, 2012, **195**, 14–21.

53 K. Tomishige, Y. Ikeda, T. Sakaihori and K. Fujimoto, *J. Catal.*, 2000, **192**, 355–362.

54 S. Huang, J. Ma, N. Zhao, M. Dong, W. Wei and Y. Sun, *Petrochem. Technol.*, 2007, **36**, 248–251.

55 Y. Zeng, Z. Ye, W. Xu, L. Chen, D. Li, L. Zhu, B. Zhao and Y. Hu, *J. Cryst. Growth*, 2005, **283**, 180–184.

56 S. S. Shinde, C. H. Bhosale and K. Y. Rajpure, *J. Photochem. Photobiol., B*, 2013, **120**, 1–9.

57 K. Sutthiumporn and S. Kawi, *Int. J. Hydrogen Energy*, 2011, **36**, 14435–14446.

58 V. E. Henrich and P. A. Cox, *The Surface Science of Metal Oxides*, Cambridge University Press, Cambridge, 1994.

59 J. Zhang and D. He, *J. Colloid Interface Sci.*, 2014, **419**, 31–38.

60 J. Robert, W. Stevens, R. V. Siriwardane and J. Logan, *Energy Fuels*, 2008, **22**, 3070–3079.

61 M. León, E. Díaz, S. Bennici, A. Vega, S. Ordõez and A. Auroux, *Ind. Eng. Chem. Res.*, 2010, **49**, 3663–3671.

62 H. Du, C. T. Williams, A. D. Ebner and J. A. Ritter, *Chem. Mater.*, 2010, **22**, 3519–3526.

63 Y.-X. Zhang, Q.-Y. Su, Z.-P. Wang, X.-Y. Gao and Z.-L. Zhang, *Wuli Huaxue Xuebao*, 2010, **26**, 921–926.

64 J. I. Di Cosimo, V. K. Díez, M. Xu, E. Iglesia and C. R. Apesteguía, *J. Catal.*, 1998, **178**, 499–510.

65 H. Noei, C. Wöll, M. Muhler and Y. Wang, *J. Phys. Chem. C*, 2011, **115**, 908–914.

66 Y. Du, L. He and D. Kong, *Catal. Commun.*, 2008, **9**, 1754–1758.

67 D. Lin-Vien, N. B. Colthup, W. G. Fateley and J. G. Grasselli, *The Handbook of Infrared and Raman Characteristic Frequencies of Organic Molecules*, Academic Press, 1991, ch. 9, pp. 129–130, 134.

68 A. Mohamadou and C. Gérard, *J. Chem. Soc., Dalton Trans.*, 2001, 3320–3328.